Available online at www.sciencedirect.com
SCIENCE DIRECT®
Acta Materialia 52 (2004) 591–600
Acta MATERIALIA
www.actamat-journals.com

Loss in coherency and coarsening behavior of Al_3Sc precipitates

S. Iwamura *, Y. Miura

Department of Materials Physics and Chemistry, Graduate School of Engineering, Kyushu University, 6-10-1 Hakozaki, Higashi-ku, Fukuoka 812-8581, Japan

Received 18 August 2003; received in revised form 18 August 2003; accepted 29 September 2003

Abstract

The coarsening behavior of the Al_3Sc particles in Al–0.2wt%Sc alloy at 673–763 K is studied on the basis of TEM observations with the numerical model. Emphasis is on the effects of coherent/semi-coherent transition of the particles. The radius for coherent/semi-coherent transition of the Al_3Sc particles is determined from TEM micrographs as 15–40 nm. The average particle radius, r_{ave}, of the Al_3Sc particles obeys the r^3_{ave} growth low both in the coherent stage ($r_{ave} < 15$ nm) and semi-coherent stage ($r_{ave} > 40$ nm). However, in the intermediate stage, where coherent and semi-coherent particles coexist ($15 < r_{ave} < 40$ nm), coarsening is delayed and particle size distribution is broadened in the experiment and also in the calculation. These results are qualitatively understood in consideration of the different growth rates of individual particles in the intermediate stage.

Keywords: Aluminum alloys; Precipitation; Phase transformation kinetics; Coherency

1. Introduction

Generally, transition elements, when added to aluminum, prefer to precipitate or crystallize as intermetallic compounds because of their poor solubility in aluminum. Therefore small addition of transition elements has large influence on the properties of Al alloys. Especially, scandium, the lightest among all transition elements, is the most prospective additive element to Al alloys for various uses. To date, it has been reported that a small amount of scandium largely improves properties of Al alloys such as strength, recrystallization temperature, microstructures and etc. [1–7]. Most of these favorable effects are mainly due to the fine dispersion of the $L1_2$–Al_3Sc precipitate, which is stable, spherical and coherent with the matrix.

The Al_3Sc phase decomposes from the α-Al supersaturated solid solution as a stable phase without forming any intermediate phases. It is thought that the coherent strain by the fairly large lattice misfit and the high antiphase boundary energy of the Al_3Sc phase contribute to disturb moving dislocations and migrating grain boundaries, and thus increase recrystallization temperature and improve microstructure stability of the alloy. Moreover, the low diffusivity and the low solubility of scandium lead to the high resistance of the Al_3Sc compounds for coarsening and keep them finely dispersed to relatively high temperatures. The Al_3Sc particle accordingly has an effect on high temperature stability of Al–Sc alloy. However, coarsening of the Al_3Sc particle cannot be avoided in the over-aging condition and deterioration of Al–Sc alloys becomes more and more serious. The knowledge of the distribution controlling and the precipitation kinetics of the Al_3Sc particles are therefore indispensable for alloy designing of Al–Sc alloys.

So far, the precipitation kinetics (nucleation, growth and coarsening) of the Al_3Sc phase in Al–Sc system have been studied by many research groups [8–12]. The Al_3Sc particle is relatively easy to study theoretically because of their homogenous precipitation and nearly spherical shape. Moreover their low volume fraction, around 1% at the most, results in large interparticle spacings in comparison with particle size. Accordingly, interaction with the neighbor particles, such as local diffusion or coherency strain surrounding each particle, is negligibly small. For this reason, the Al–Sc system has been often used as the test alloy system for the inspection of

* Corresponding author. Tel.: +81-926-424147; fax: +81-926-320434.
E-mail address: shingo.iwamura@ma9.seikyou.ne.jp (S. Iwamura).

1359-6454/$30.00 © 2003 Acta Materialia Inc. Published by Elsevier Ltd. All rights reserved.
doi:10.1016/j.actamat.2003.09.042

precipitation kinetics. Hyland [8] reported that nucleation of the Al_3Sc precipitates is explained reasonably by the classical nucleation theory. As for the coarsening of the Al_3Sc particles in Al–Sc alloys including sufficient amount of scandium, what is consistent with the theory of interfacial-energy driven coarsening established by Lifshits, Slyozov and Wagner (LSW theory) [13,14], the well-known $r_{ave}^3 = kt$ law, have been reported by Marquis et al. [9] and Novotny et al. [10] individually. Recently, Robson and coworkers [12] generally succeeded in the quantitative prediction of the evolution of Al_3Sc particle size distribution (PSD) at whole stages of transformation, nucleation, growth and coarsening, by using Kampmann and Wagner numerical (KWN) model [15], which gathered up the kinetics of nucleation and growth numerically.

However, interfacial state of the Al_3Sc particles changes from coherent to semi-coherent with its growth and it is suggested that particle coherency plays an important role in their coarsening behavior. For instance, Drits and coworkers [11] stated that the coarsening rate of the Al_3Sc particles increases by the coherency disappearance, indicating that it promotes the increase in particle spacing and leads to the deterioration of Al–Sc alloys in over-aging conditions. It is also expected that the coherency loss of the Al_3Sc particles effects on the interaction between the particles and moving dislocations and migrating grain boundaries. The critical radius where a particle begins to loose coherency in growth process, has been reported to be about 20 nm [3,9,11]. As for the condition where coherent particles and semi-coherent particles coexist, certain modifications should be made to the coarsening kinetics, because the Al/Al_3Sc interfacial energy, σ, cannot be uniquely defined.

In the present investigation, the effect of particle coherency on coarsening process of the Al_3Sc particle at high temperature in the Al–0.2wt%Sc alloy is studied by TEM analysis, and the KWN model is modified based on the results of TEM observation with emphasis on the coherency change during growth. Coarsening behavior of the Al_3Sc particle is successfully understood by the use of a numerical model.

In Sections 2 and 3, the experimental methods and the results will be shown. In Section 4, numerical calculations were made on the basis of the KWN model and the experimental results, and discussion will be made on the calculation results in comparison with the experimental results.

2. Experiment

2.1. Experimental procedure

The cast ingot of Al–0.2(mass%)Sc alloy, the composition of which is shown in Table 1, was hot-rolled and cold-rolled to 3 mm thick plate. Rectangular specimens, $3 \times 3 \times 6$ mm^3, were cut out from the plate. After encapsulated in glass tubes with Ar gas, the specimens were solution treated for 2 h at 913 K, and quenched into iced water. The specimens were subjected to aging at 673–763 K for 10^3–10^6 s to obtain the equilibrium Al_3Sc phases. Thin plates of 300 μm thickness were cut out from the specimens, and thin foils for TEM observation were prepared by twin-jet electropolishing at 263 K with a solution of 30% nitric acid and 70% methanol.

Table 1
Chemical composition of the specimens (wt%)

Si	Fe	Cu	Mg	Sc	Al
<0.01	<0.01	0.0012	–	0.20	Balance

These foils were examined by using the transmission electron microscope, JOEL-200CX, of the HVEM Laboratory of Kyushu University. The average particle radius, r_{ave}, and PSD were measured from dark field (DF) images taken by the $L1_2$ superlattice reflections. To obtain statistically reliable data, 200–1000 particles were analyzed on more than three micrographs for each aging condition. The coexistence of coherent particles and semi-coherent particles was often encountered in the specimens aged at 733 K. And for these specimens, PSD, and also the ratio of semi-coherent particles was determined from a pair of DF image and BF image from the same region. The details of the principle and process for the judgment of particle coherency are described in Section 2.2.

2.2. The method of judging the coherency of the particles

In general, the most reliable information of coherency between a particle and the matrix is obtained from HREM analysis, although it is not easy to analyze many particles at a time. In this work, particle coherency was judged from Ashby and Brown (AB) contrast [17] which appears around a spherical coherent particle in BF images under the just Bragg condition. So-called no-contrast line appears in normal direction to the $\boldsymbol{g}$ vector. Loss of spherical strain caused by the introduction of interfacial dislocations is detected by the irregularity of the no-contrast line. Though strict judgment for all particles is technically difficult, a large number of particles can be analyzed by using AB contrasts. What has to be noticed is that BF images should be taken at the condition of $s_g = 0$, where lattice distortion is reflected most sensitively. Irregularity of no-contrast line appeared at the $s_g = 0$ is possibly disappear at $s_g \neq 0$. An example is shown in Fig. 1 for coherency judgment. Overlapped contrasts were excluded from the analysis because of their uncertainty. Asymmetrical AB contrasts

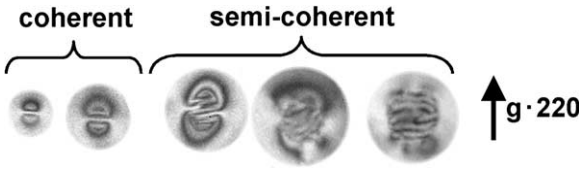

Fig. 1. Contrasts from coherent and semi-coherent particles. Coherency of the particles is judged from the symmetry of the spherical strain contrasts.

from the particles near the foil surface [17] were also neglected because the contrasts are influenced by strain relaxation at foil surfaces.

3. Results

3.1. Coherency between the Al_3Sc particle and the Al matrix

The homogeneous dispersion of the Al_3Sc precipitates is confirmed by DF images shown in Fig. 2. Though cauliflower-like shaped particles as were reported by Marquis [9] and Novotny [10] were also observed in the condition of 673 K – 10^3 s (the lowest temperature and the shortest time in the present work), the observed Al_3Sc particles were generally spherical

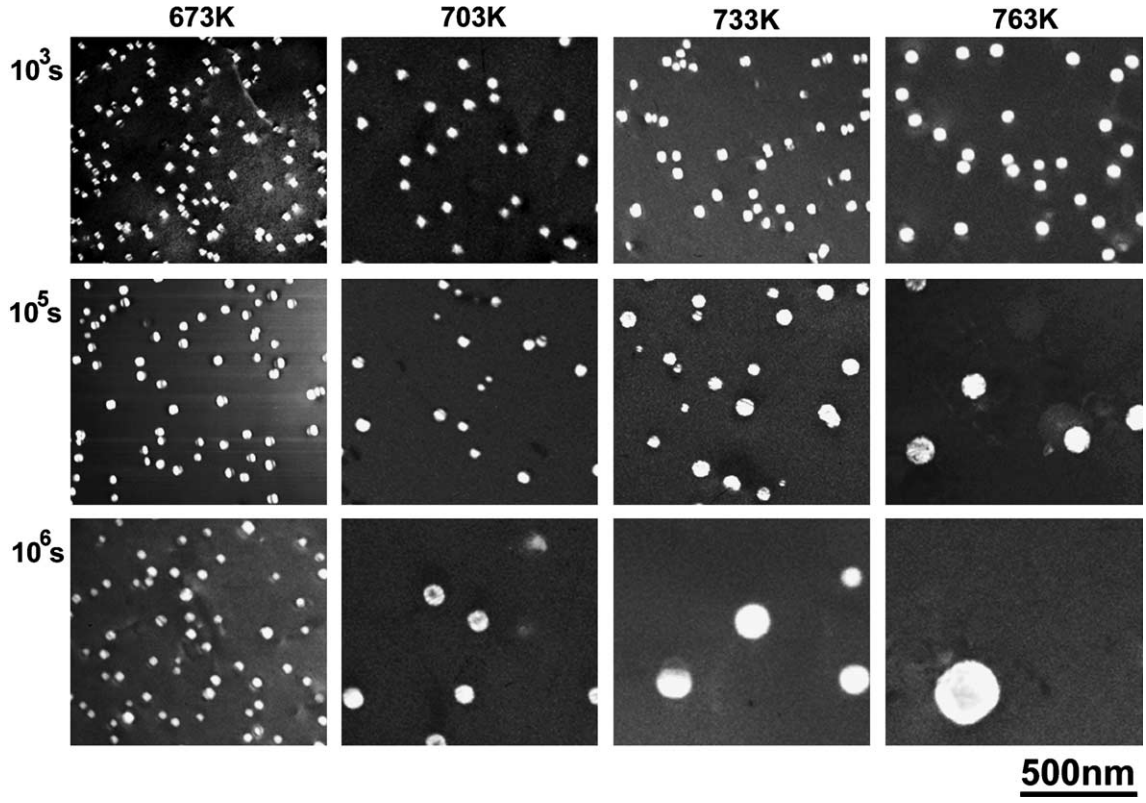

Fig. 2. The centered dark field images of the Al_3Sc particles in Al–0.2Sc alloy for several aging conditions.

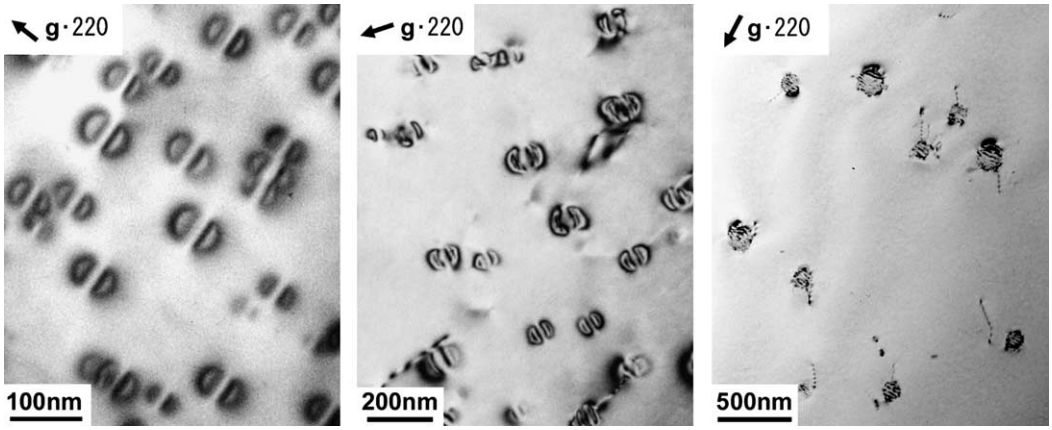

Fig. 3. The bright field images of the Al_3Sc particles for different aging conditions: (a) 673 K, 3×10^5 s, (b) 703 K, 5×10^5 s, (c) 733 K, 10^6 s.

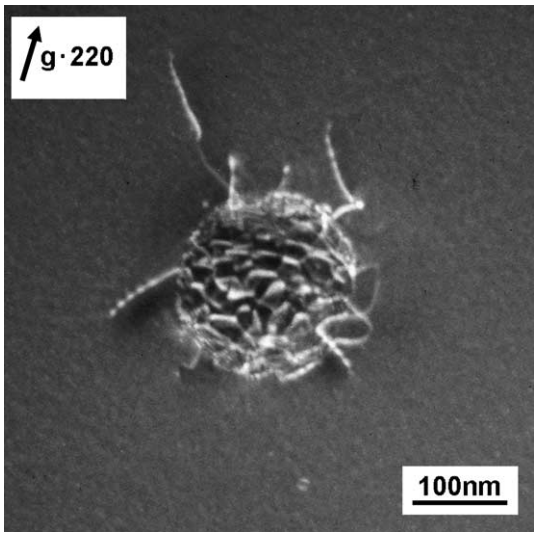

Fig. 4. Weak beam image of dislocation network surrounding an Al_3Sc particle at the Al/Al_3Sc interface.

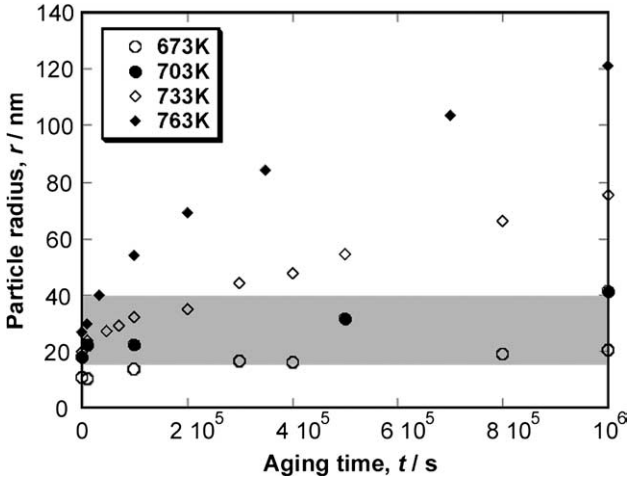

Fig. 5. Average particle radius of the Al_3Sc particles as a function of aging time for different aging temperatures: (a) 673 K, (b) 703 K, (c) 733 K and (d) 763 K for 10^3–10^6 s. The Al_3Sc particles loose their coherency in the radius range from 15 to 40 nm (shaded area).

under the present aging conditions. AB contrasts in BF images (Fig. 3) become irregular on aging, suggesting that coherency begins to break down in accordance with particle growth. The semi-coherent Al_3Sc particles co-existed with coherent particles in the particle radius range from 15 to 40 nm. Fig. 4 shows the weak beam (WB) image of the semi-coherent particle. The complicated dislocation networks at the Al/Al_3Sc interface never disappeared in the WB images obtained by using several different $\boldsymbol{g}$ vectors. This suggests that the networks are formed three-dimensionally at the Al/Al_3Sc interface and they consist of dislocations with several different Burgers vectors. In this condition, there were no apparent change between the $L1_2$ superlattice diffraction pattern relative to the initial state, where there is perfect coherency between the particle and the matrix. This indicates that the particles are not incoherent, but were semi-coherent.

3.2. Coherency loss and coarsening of the Al_3Sc particle

Hyland reported that the number density of Al_3Sc particles began to decrease from 8000 s at 561 K and from 1000 s at 616 K in Al–0.18wt%Sc alloy [8]. The temperatures employed in the present work, 673, 703, 733 and 763 K, are closer to the nose temperature of TTT curves (around 723 K [12,19]) than that in Hyland's report. It is, therefore, reasonable to assume that precipitation of the Al_3Sc phase is completed and coarsening starts at 10^3 s in the present Al–0.2wt%Sc alloy at temperatures 673–763 K. Fig. 5 shows the observed average radius of the Al_3Sc particles as a function of aging time for each aging temperature. In the following discussion, the precipitation process is divided into three stages: (1) coherent stage ($r_{ave} < 15$ nm), with almost all the particles coherent, (2) intermediate stage ($15 < r_{ave} < 40$ nm), with coexisting coherent and semi-coherent particles, (3) semi-coherent stage ($r_{ave} > 40$ nm), with almost all the particles semi-coherent. It should be noted that these stages are defined on the basis of average particle radius.

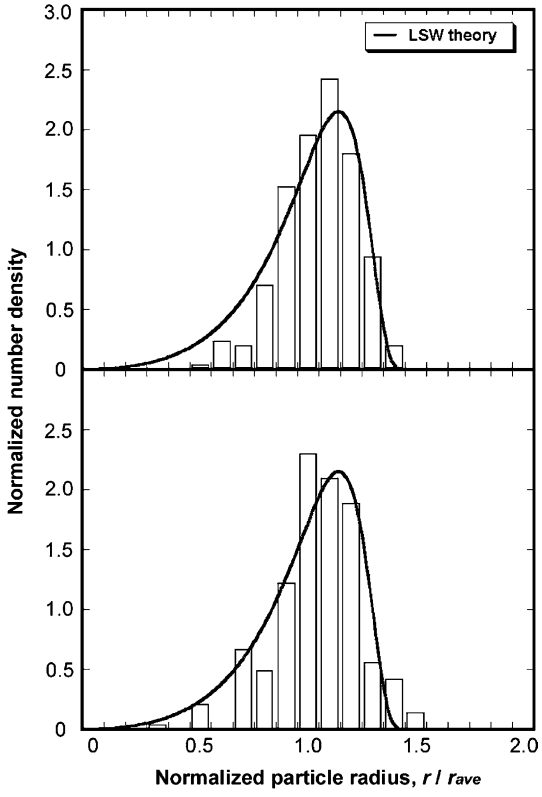

Fig. 6. PSD for the Al_3Sc particles: (a) aged at 673 K for 3×10^5 s and (b) aged at 763 K for 3.5×10^4 s.

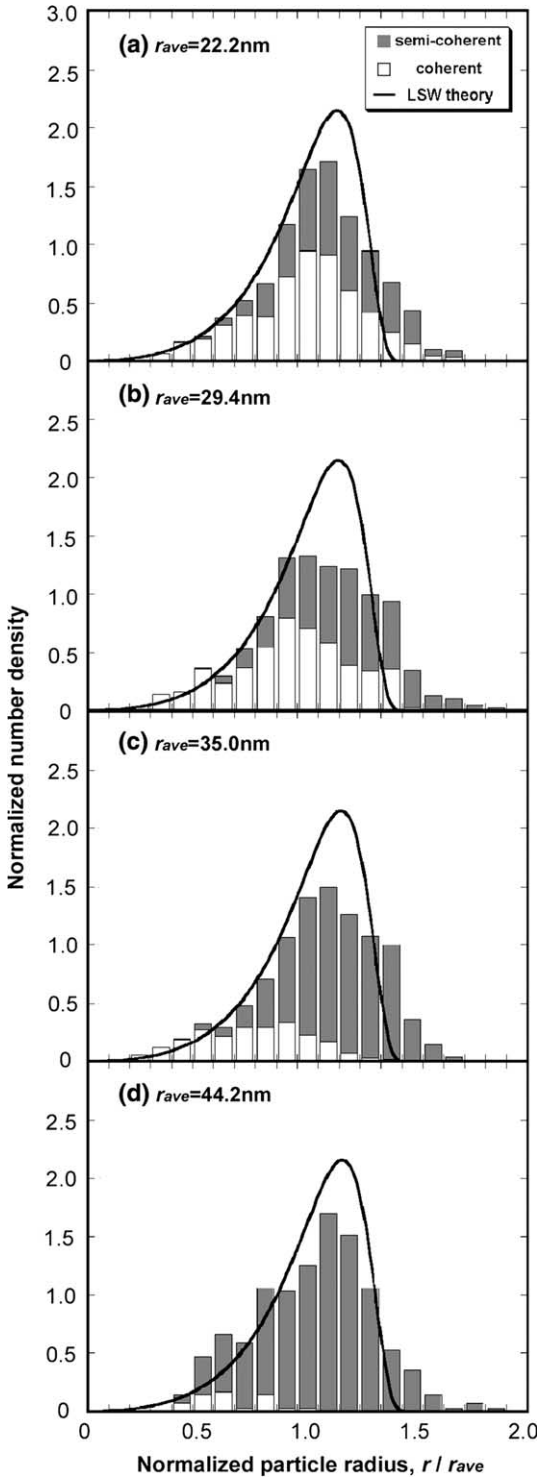

Fig. 7. PSD for the Al_3Sc particles: aged at 733 K for (a) 10^4 s, (b) 7×10^4 s, (c) 2×10^5 s and (d) 3×10^5 s.

On aging at 673 K, the Al_3Sc particles began to loose their coherency from around 3×10^5 s. The coherent and the semi-coherent particles coexisted at 703 K for 10^3–10^6 s. At 733 K, the coarsening process is in the intermediate stage, though the progress to semi-coherent stage occurred after 3×10^5 s. At 763 K, the particles became semi-coherent at the early stage of coarsening, e.g., at 10^4 s.

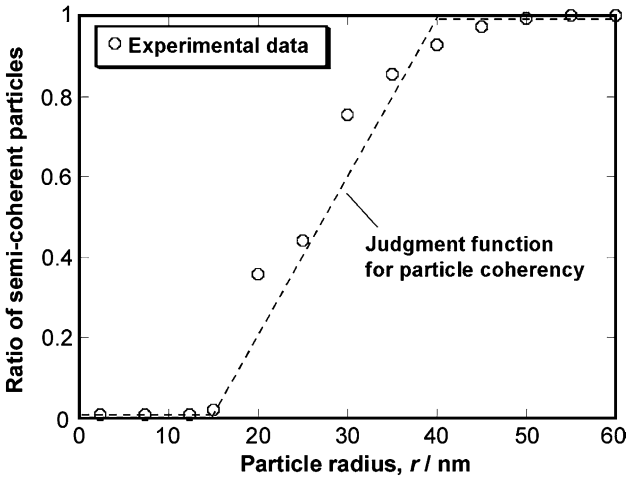

Fig. 8. The ratio of the number of semi-coherent particles to the total number of the particles at each radius column at 733 K. The linear relationship shown by a dashed line in the figure is used for the present numerical calculation.

The PSDs in the coherent stage and semi-coherent stage were comparable with the ideal distribution expected from the LSW theory (Fig. 6). However, as seen in Fig. 7, which shows the evolution of PSD combined with distinction of coherent and semi-coherent at 733 K, PSDs became broader than the ideal in the intermediate stage. As shown in Fig. 8, the ratio of semi-coherent particles at each radius column rapidly increases from around 15 to 40 nm, and no clear dependence on temperature and time was observed.

4. Discussion

4.1. The radius for coherent/semi-coherent transition of the Al_3Sc particles

Al_3Sc particles seem to loose their coherency in the radius range from 15 to 40 nm in coarsening stage as described in the preceding section. It is desirable to mention about the radius for coherent/semi-coherent transition, r_t, of the Al_3Sc particles before discussing about coarsening behavior.

As shown in Figs. 3(c) and 4, Al/Al_3Sc interfacial dislocations do not protrude to the matrix. These observations suggest that dislocations in matrix do not participate in the processes of coherency change. Therefore it is thought that the driving force for the formation of interfacial dislocations mainly arises from the elastic energy caused by the lattice misfit. When the particle coherency is lost, the total energy of the matrix containing a particle will be conserved. In other words, the increase of interfacial energy by the introduction of

dislocations is equal to the decrease of elastic energy by the relaxation of lattice distortion. Thus, the following relationship [20] is valid at radius for coherent/semi-coherent transition,

$$4\pi r_t^2 \sigma_{dis} = 8\pi r_t^3 G\delta^2 \frac{(1+\upsilon)}{3(1-\upsilon)}, \quad (1)$$

where G and υ are shear modulus and Poisson ratio of the matrix, respectively, and δ is lattice misfit between the particle and the matrix, σ_{dis} is the energy of interfacial dislocation network per unit area. According to Jesser et al. [20], σ_{dis} is expressed as follows:

$$\sigma_{dis} = \frac{Gb}{2\pi^2}\left\{1+\beta-\left(1+\beta^2\right)^{1/2}-\beta\ln\left(2\beta\left(1+\beta^2\right)^{1/2}-2\beta^2\right)\right\}, \quad (2)$$

$$\beta = \frac{\pi\delta'}{(1-\upsilon)}, \quad (3)$$

where b is the magnitude of the Burgers vector and δ' is the decrease in lattice misfit by the introduction of interfacial dislocations. In the present case of Al matrix and Al_3Sc particle, substitution of $G = 26.2$ Gpa, $b_{110} = 0.286$ nm, $\delta' = +0.013$ (calculated from the lattice constant of Al and Al_3Sc) and $\upsilon = 1/3$ in Eqs. (2) and (3) produces $\sigma_{dis} = 0.073$ J/m^2. The critical transition radius for the coherency loss is given as $r_t = 12.3$ nm by the combination of Eq. (1) and the estimated value of σ_{dis}. The practical particle size for coherency loss is expected to be larger than the above calculated value, since the activation energy for the outbreak of interfacial dislocations is necessary. Accordingly, the calculated value of critical transition radius ($r_t = 12.3$ nm) is reasonable as compared to the measured minimum value of r_t (15 nm). The scatter in the measurement of transition radius in Fig. 8, 15–40 nm, indicates that there is a difference in time for individual Al_3Sc particles to start loosing coherency. The difference may partly come from diffusional or elastic interaction between neighboring particles. However these reasons seem to be not so important because of the large interparticle spacing between Al_3Sc particles. In any case, dependence of the transition radius, r_t, on time and temperature is not suggested from the present experimental data. There is room opened for further investigation on this point.

4.2. Coherency loss and coarsening of the Al_3Sc particles

4.2.1. Prediction of coarsening behavior

To interpret the coarsening behavior, including intermediate stage, of the present Al_3Sc particles, the KWN model [15] was modified on the basis of the present experimental data shown in Section 3. In the KWN model, nucleation, growth and coarsening are treated as coupled processes, so that they can be numerically simulated. The details of the KWN model will not be reviewed here. The studies by Kampmann and his coworkers should be referred [15]. The present numerical calculation for the coarsening process of the Al_3Sc precipitates requires the following conditions:

- The particles are in equilibrium of perfect spherical shape and the diffusion field around particles is in stable state. Interparticle interaction (diffusion or elastic strain) between neighbor particles is negligible.
- Both coherent interface and semi-coherent interface have isotropic homogeneous energies.
- The dislocations protruded from semi-coherent interface are negligible and do not affect on the diffusion of solute scandium.
- The ratio of semi-coherent particles to the total depends only on the particle radius, and has no dependence on time and temperature of the annealing. The change of diffusion field according to conversion of coherency settles down in an instant.

Under the above conditions, the growth rate of individual particles is given by [16]

$$\frac{dr}{dt} = \frac{D}{r}\frac{C-C_r}{C_\beta - C_r}, \quad (4)$$

where r is particle radius, D is diffusion constant of solute scandium in the matrix, C_β is equilibrium concentration of solute scandium in the particle phase and C is mean field concentration at the point of time. The equilibrium concentration of solute scandium at the Al/Al_3Sc interface in the matrix, C_r is given by [21]

$$C_r = C_\alpha \exp\left(\frac{2\sigma V(1-C_\alpha)}{rk_B T(C_\beta - C_\alpha)}\right), \quad (5)$$

where V is the atomic volume of solute in the particle phase, k_B is Boltzmann constant, σ is the interfacial energy, and C_α is equilibrium concentration of solute scandium in the matrix. As shown by Eq. (5), C_r depends on interfacial energy. Therefore, growth (shrinking) rate varies according to whether the interfacial is coherent or not.

To make a prediction of the time evolution of PSD, continual time and radius spaces were divided into discreet time steps and radius columns. The growth rate of the particle was decided from Eq. (4) at each time step and at each radius column. The feature of this calculation is that the ratio of semi-coherent particles to all particles was determined for each radius column on the basis of experimental data shown in Fig. 8. The PSD is updated by using growth rate distinguished by interfacial condition and used to recalculate the scandium concentration in the matrix by using the mean field approximation. By repeating these steps, time evolution of the PSD was predicted. If initial PSD and solute concentration were given, information about various parameters (average particle radius, particle number density, volume fraction of particles, solute concentra-

tion in the matrix, etc.) can be calculated for different temperatures.

Table 2 shows the data used for the present numerical calculations. To make calculation for the coarsening stage, initial condition was adopted as the state where almost all of supersaturated scandium decomposes to form Al_3Sc phase. The nucleation of the new Al_3Sc particles was negligible in this condition. Initial solute content was decided as $C = (C_\alpha - C_0) \times 0.95$, where C_0 is the scandium concentration in the alloy. The particular choice of 0.95 is likely not critical because solute concentration settles on steady state within comparatively short time. The ideal LSW distribution was adopted as initial PSD, and the initial average particle radius was chosen as $r_{ave} = 10$ nm, where all particles are coherent (Note: In the ideal LSW distribution, radius of the coarsest particle is 1.5 times of r_{ave}. 15 nm, 1.5 times of 10 nm, is equal to the observed minimum transition radius). In the completion of the numerical calculation, the predicted curves were shifted so as to be consistent with the experimental result at the time of 10^3 s to adjust the difference of initial r_{ave}.

4.2.2. Comparison of calculated results with experimental results

To match calculation results with experimental data, we chose coherent interfacial energy, σ_1, and semi-coherent interfacial energy, σ_2, in such a way that the difference between the calculation and the experiment is minimized. This procedure is similar to the conventional determination of particle–matrix interfacial energy by fitting the diffusional controlled growth law, $r_{ave}^3 = kt$, with the experimentally determined rate constant, k [21]. Temperature dependence of σ is neglected in the present calculation, because Asta reported that Al/Al_3Sc interface energy predicted by the first-principle calculation has little temperature dependent (around 5%) below 800 K [22]. The best fit between the calculated and the experimental was found at $\sigma_1 = 0.12$ J/m^2 and $\sigma_2 = 0.17$ J/m^2, and these values are in good agreement with those previously reported: $\sigma = 0.078$–0.125 J/m^2 (546–616 K, Hyland [8]), $\sigma = 0.041$–0.063 J/m^2 (673–733 K, Jo and Fujikawa [23]), $\sigma = 0.105$ J/m^2 (623 K, Novotny and Ardell [10]) and $\sigma = 0.192$ or 0.226 J/m^2 (0 K, {1 0 0} or {1 1 1} interface, Asta [22]). Furthermore, the value of $\sigma_2 - \sigma_1$ (0.05 J/m^2) is comparable with the calculated σ_{dis} (0.072 J/m^2) as shown in Section 4.1. This implies that the chosen values of σ_1 and σ_2 are reasonable to some extent.

The calculated time evolution of r_{ave} shown in Fig. 9 is in conformity with the experimental data. In the coherent stage, coarsening curve becomes linear in r_{ave}^3–t plot, and coarsening rate, k, slightly decrease from coherent stage to the intermediate stage as is shown in Fig. 9(a) for 673 K. Coarsening rate increases from the intermediate stage to semi-coherent stage, as is clearly recognized at 733 K (Fig. 9(c)). In the semi-coherent stage, coarsening rate approaches asymptotically to a fixed value, larger than that in coherent stage. As for the coherent stage and the semi-coherent stage, coarsening behavior seems to be explained by the r^3–t growth law. It is noteworthy that the coarsening is always delayed in the intermediate stage. It can be understood qualitatively in consideration of the different growth rates of individual particles in the intermediate stage. The growth rate of a particle, given by Eq. (4), becomes to zero in the equilibrium state ($C_r = C$) of solute at interface. The critical radius for growth, r_c, is derived from Eq. (5) as follows, corresponding to the minimum size with which a particle can grow.

$$r_c = \frac{2\sigma V(1 - C_\alpha)}{k_B T(C_\beta - C_\alpha)} \left(\ln \frac{C}{C_\alpha}\right)^{-1}. \tag{6}$$

The equation indicates that the critical radius for semi-coherent particles is (σ_2/σ_1) times larger than that for coherent particles. What is important here is the tendency that semi-coherent particles need larger critical radius to grow than that for coherent particles. Therefore, the particles whose radius, r, is in the range of $r_{c1} < r < r_{c2}$ are possible to grow or shrink depending on their coherency. In other words, in this region, the coherent particles grow but the semi-coherent particles shrink, thus the increase in average particle radius is disturbed. This consideration leads to an expectation that loss in coherency is not always connected directly with promotion of coarsening. When r_{c1} becomes larger than 40 nm, all particles in the range of $r < 40$ nm will shrink, regardless of their coherency.

Table 2
Parameters and their values used in the calculations

T (K)	673	703		733	763
C[a] (–)	0.00955	0.0154		0.0238	0.0358
D[b] (m^2/s)	1.98×10^{-17}	7.42×10^{-17}		2.49×10^{-16}	7.61×10^{-16}
C_β (–)			0.25		
V[c] (m^3/mol)			1.388×10^{-5}		

[a] C_α is calculated from the solid solubility equation: $C_\alpha = \exp(\Delta S/R)\exp(-\Delta H/RT)$, where ΔS is the change of entropy, ΔH is the enthalpy change. The value of $\Delta S/R$ and ΔH is taken as 6.57 (–) and 62.8 (kJ/mol) respectively [23].

[b] D is calculated from the formula: $D = D_0 \exp(-E_D/RT)$. The value of D_0 and E_D is taken as 5.31×10^{-4} (m^2/s) and 173 (kJ/mol) respectively [25].

[c] V, the partial molar volume of Sc in Al_3Sc phase, is estimated from the molar volume of Al_3Sc ($= 4.16 \times 10^{-5}$ (m^3/mol)) taking a difference of atomic radius between Al and Sc into consideration.

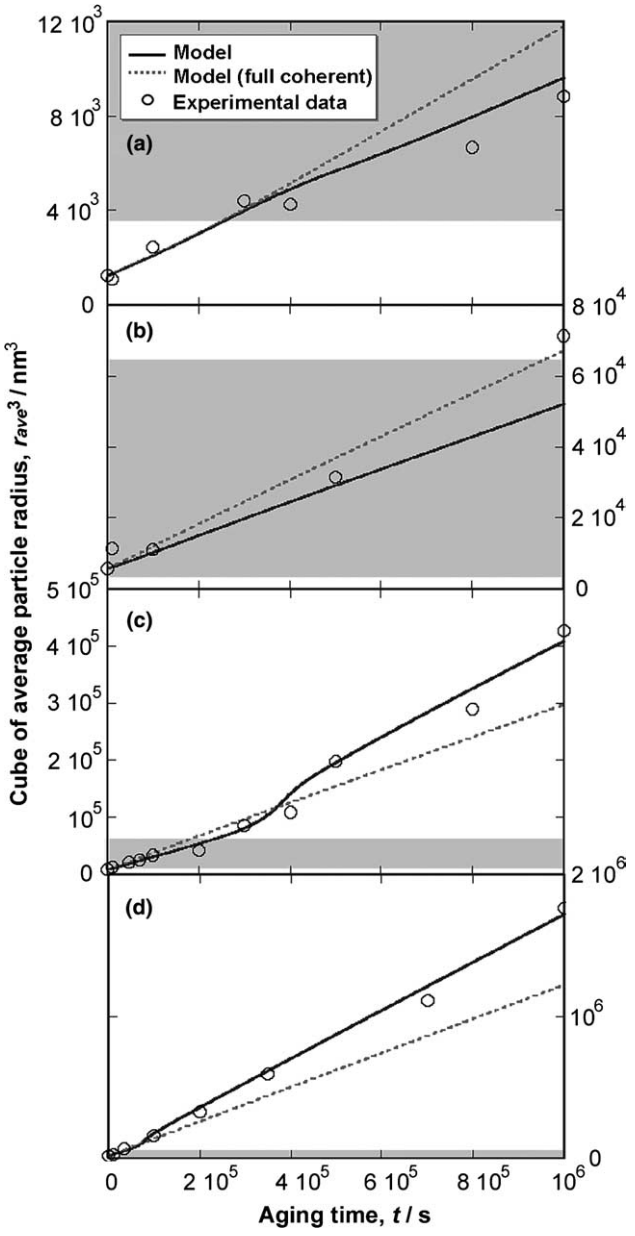

Fig. 9. Variation of particle size with aging time (10^3–10^6 s) for different aging temperatures: (a) 673 K, (b) 703 K, (c) 733 K and (d) 763 K. The shaded areas in the figures indicate the coherent/semi-coherent transition range (15–40 nm)

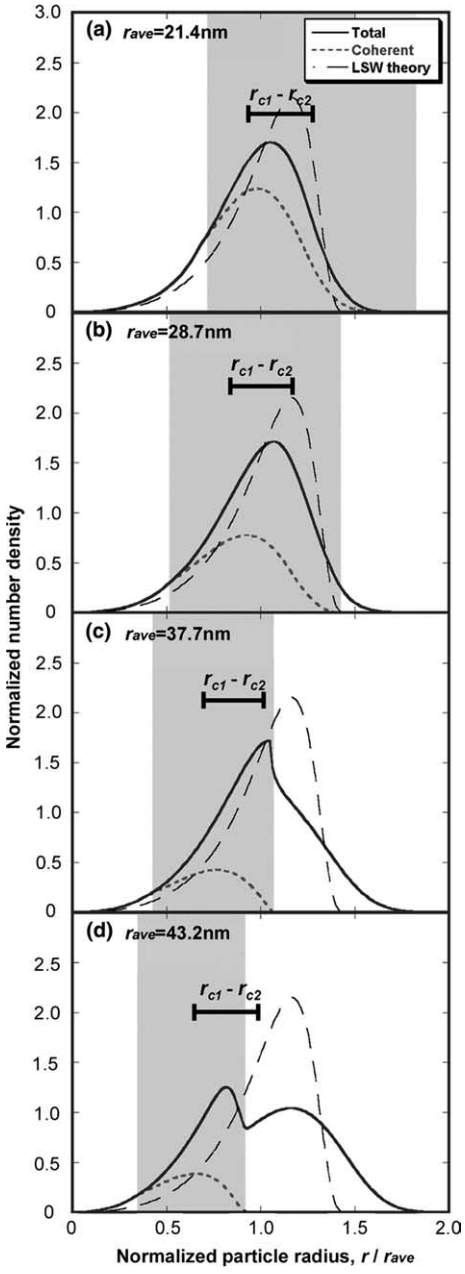

Fig. 10. Predicted PSD for the Al_3Sc particles aged at 733 K for (a) 10^4 s, (b) 7×10^4 s, (c) 2×10^5 s and (d) 3×10^5 s. Shaded area means transition region form 15 to 40 nm.

The calculated PSDs in the intermediate stage (in the same condition as in Fig. 7) are shown in Fig. 10. The broadening of PSD is confirmed not only in experiment (Fig. 7) but also in calculation (Fig. 10), suggesting that it comes from the presence of the radius range which delays coarsening in the intermediate stage. In addition, the predicted PSDs (Fig. 10) indicate clearly an inflection point at 40 nm and a remarkable increase in the predicted coarsening rate is also observed at the beginning of the semi-coherent stage from intermediate stage (Fig. 9(c)). These features may come from the assumed liner relationship between the semi-coherent ratio and radius in the range of 15–40 nm (Fig. 8). The remarkable change at 40 nm in predicted PSDs is expected to become smoother in practical cases.

4.3. Deterioration of Al–Sc alloys caused by coherency loss of Al_3Sc particles

Loss in particle coherency promotes the increase in coarsening rate and interparticle spacing, and also produces the decrease in the pinning forces caused by particles on migrating grain boundaries and on moving dislocations. In the intermediate stage, the decrease in

the pinning effects of the Al_3Sc particles occurs with the progress of coherency loss. On entering the semi-coherent stage, the enhanced coarsening leads to accelerated increase in interparticle spacing. Fig. 11 shows the calculated ratio of semi-coherent particles to all the particles as a function of aging time. The promotion of increase in particle spacing was expected to starts at around 85%, which roughly shows the border between the intermediate stage and the semi-coherent stage. The calculated 85% limit of coherency loss of the Al_3Sc particle in Al–0.2Sc at 673–763 K is shown in Fig. 12. Above the limit, the favorable effects by the Al_3Sc particles will rapidly deteriorate.

The effect of other elements on particle coherency is also important, because Sc is often used as a supporting additive together with other main elements for Al alloys. The misfit between the Al_3Sc particles and the Al matrix is possibly changed by solution of other elements in the Al matrix, and also in the Al_3Sc particles as Harada suggested [24]. The authors have reported that addition of 3.0 wt% magnesium highly improves the coherency of the Al_3Sc particles and makes the transition radius larger to 40–80 nm [18]. The change in degree of coherency will have large influence on the transition radius and the coarsening behavior.

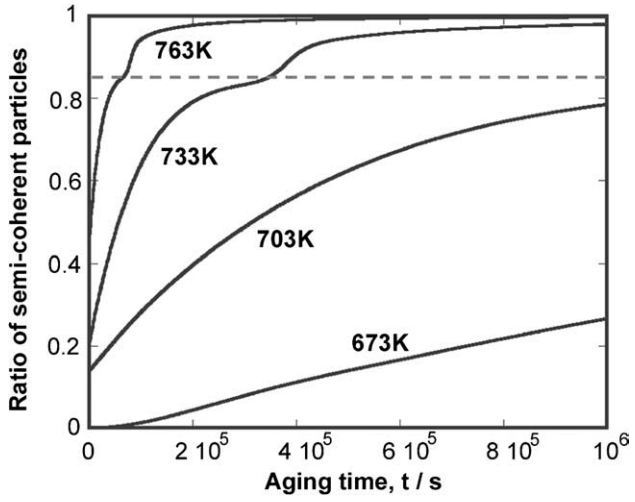

Fig. 11. Change in predicted semi-coherent ratio with time. Dashed line means 85% coherency limit to switch over from transition stage to semi-coherent stage.

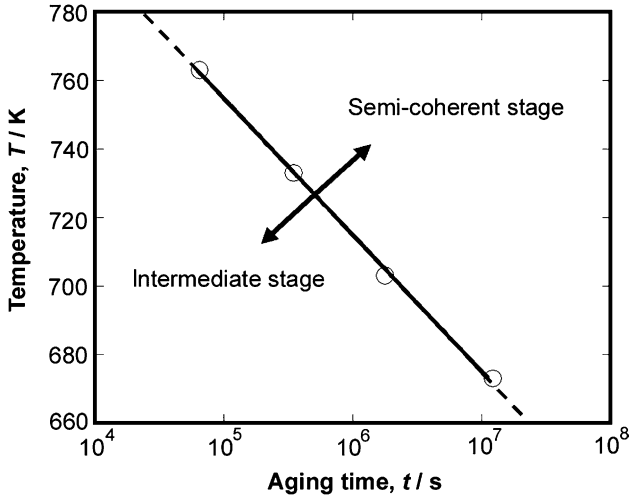

Fig. 12. Predicted 85% coherency limit of the Al_3Sc particle in Al–0.2Sc alloy.

5. Conclusion

The correlation between the coarsening behavior and coherency of the Al_3Sc particles in the Al–0.2wt%alloy was investigated based on TEM observations and the calculation using numerical model. Emphasis was on the effects of coherent/semi-coherent transition of the particles. The results are summarized as follows:

- The radius for coherent/semi-coherent transition of the Al_3Sc particle was determined as 15–40 nm from the TEM analysis. Distinct dependence of the transition radius on temperature and time was not observed.
- By fitting the predicted curves from a numerical model to the experimental results, the energy of the Al/Al_3Sc interface was estimated as 0.12 J/m^2 (σ_1) for coherent interface and 0.17 J/m^2 (σ_2) for semi-coherent interface. The difference between two value, 0.05 J/m^2 (σ_{dis}), is regarded as the energy due to interfacial dislocation. These values are in good agreement with those previously reported.
- The average particle radius, r_{ave}, of the Al_3Sc particles obeys the r_{ave}^3 growth low both in the coherent stage ($r_{ave} < 15$ nm) and semi-coherent stage ($r_{ave} > 40$ nm), and the coarsening rate in semi-coherent stage is larger than that in coherent stage. However, the coarsening of the Al_3Sc particles is delayed in the intermediate stage ($15 < r_{ave} < 40$ nm), where coherent and semi-coherent particles coexist.
- It is suggested that the Al_3Sc particle is delayed in its coarsening in the radius range, $r_{c1} < r < r_{c2}$, where r_{c1} is the critical radius for growth of coherent particles and r_{c2} is that for growth of semi-coherent particles. Both r_{c1} and r_{c2} are dependent on time and temperature.

Acknowledgements

The authors would like to acknowledge the financial support of the Light Metals Educational Foundation, Osaka, Japan.

References

[1] Toropova LS, Eskin DG, Kharakterova ML, Dobatkina TV. Advanced aluminum alloys containing scandium. Gordon and Breach Science Publishers; 1998.
[2] Seidman DN, Marquis EA, Dunand DC. Acta Met 2002;50:4021–35.
[3] Jones MJ, Humphreys FJ. Acta Met 2003;51:2149–59.
[4] Parker BA. Mater Sci Forum 1995;189:347.
[5] Miura Y, Nakayama M, Furuta A. In: Proceedings of the Seventh JIM International Symposium on Aspect of High Temperature Deformation and Fracture in Crystaline Materials; 1993. p. 28–31.
[6] Miura Y, Shioyama T, Hara D. Mater Sci Forum 1996;217–222:505–10.
[7] Nakayama M, Furuta A, Miura Y. Mater Trans JIM 1997; 38(10):852–7.
[8] Hyland Jr RW, Stiffler RC. Scripta Mater 1991;24:473.
[9] Marquis EA, Seidman DN. Acta Met 2001;49:1909–19.
[10] Novotny GM, Ardell AJ. Mater Sci Eng A 2001;318:144–54.
[11] Drits MY, Ber LB, Bykov YG, Toropova LS, Anastaseva GK. Phys Met Metall 1984;57(6):118.
[12] Robson JD, Jones MJ, Prangnell PB. Acta Met 2003;51:1453–68.
[13] Wagner CZ. Electrochemistry 1961;65:581.
[14] Lifshitz IM, Slyozov VV. Phys Chem Solids 1961;19:35.
[15] Wagner R, Kampmann R. Mater Sci Technol 1991;5:213–303.
[16] Ratke L, Voohees PW. Growth and Corsening. Berlin: Springer; 2002. p. 67.
[17] Ashby MF, Brown LM. Phil Mag 1963;8:1083.
[18] Iwamura S, Nakayama M, Miura Y. Mater Sci Forum 2002;396–402:1151–6.
[19] Zakharov VV. Met Sci Heat Tr 1997;39:61–6.
[20] Jesser WA. Phil Mag 1968;19:993–9.
[21] Calderon HA, Voorhees PW. Acta Met 1994;42:991.
[22] Asta M, Foiles SM, Quong AA. Phys Rev 1998;57B:11265.
[23] Jo HH, Fujikawa S. Mater Sci Eng A 1993;171:151.
[24] Harada Y, Dunand DC. Scripta Met 2003;48:219–22.
[25] Fujikawa S. Defect Diffusion Forum 1997;143–147:114.